Approximating Road Geometry with Multisine Signals for Driver Identification

Kolff, Maurice J.C.; Van Der El, Kasper; Pool, Daan M.; Van Paassen, Marinus M.; Mulder, Max

DOI
10.1016/j.ifacol.2019.12.082

Publication date
2019

Document Version
Final published version

Published in
IFAC-PapersOnline

Available online at www.sciencedirect.com

ScienceDirect

IFAC Papers Online CONFERENCE PAPER ARCHIVE

IFAC PapersOnLine 52-19 (2019) 341–346

Approximating Road Geometry with Multisine Signals for Driver Identification

Maurice J. C. Kolff, Kasper van der El, Daan M. Pool, [1] **Marinus M. van Paassen, and Max Mulder**

Control and Simulation, Faculty of Aerospace Engineering, TU Delft, 2629 HS, Delft, The Netherlands

Abstract: The understanding of human responses to visual information in car driving tasks requires the use of system identification tools that put constraints on the design of data collection experiments. Most importantly, multisine perturbation signals are required, including a multisine road geometry, to separately identify the different driver steering responses in the frequency domain. It is as of yet unclear, however, to what extent drivers steer differently along such multisine roads than they do for real roads. This paper presents a method for approximating real-world road geometries with multisine signals, and applies it to a stretch of road used in an earlier investigation into driver steering. In addition, a human-in-the-loop experiment is performed to collect driver steering data for both the realistic real-world road and its multisine approximation. Overall, the analysis of driver performance metrics and driver identification data shows that drivers adopt equivalent control behaviour when steering along both roads. Hence, the use of such multisine approximations allows for the realization of realistic roads and driver behaviour in car driving experiments, in addition to supporting the application of quantitative driver identification techniques for data analysis.

Keywords: manual control, driving, multisine signals, system identification, driver modeling

1. INTRODUCTION

Much of our understanding of driver visuomotor steering behavior in lane keeping tasks is based on models (Donges, 1978; McRuer et al., 1977; Steen et al., 2011; Van der El et al., 2019a). The parameters of driver models can be estimated directly from experimental steering data, using *system identification* techniques. Such model parameters explicitly quantify control processes that are *internal* to the driver, such as their visual response delay, look-ahead time, and feedback and feedforward control gains. Unfortunately, this approach by definition requires that a model is already available, and the insight gained from the estimated parameters depends profoundly on the model's ability to capture the driver's steering dynamics.

Black-box system identification techniques can be applied to measure drivers' steering dynamics, without assuming a model *a priori*. For example, Van der El et al. (2019a) obtained Frequency Response Function (FRF) estimates of drivers' separate responses to road preview, vehicle lateral position and vehicle heading, and proposed a novel, physically interpretable, driver steering model in accordance with each observed steering response.

Unfortunately, the application of such frequency-domain identification techniques requires a driving experiment where the road centerline trajectory is defined according to a *multisine* signal. It is currently unclear, however, to what extent the multisine road signals used by Van der El et al. (2019a) match real-world roads and evoke realistic driver steering behavior.

[1] Corresponding author: d.m.pool@tudelft.nl

This paper investigates to what extent driver steering behavior on multisine roads is identical to steering along a winding real-world road. To do so, first, a method is introduced for approximating a real-world road trajectory as accurately as possible by a multisine signal. This method is then applied to obtain a multisine approximation of the road used in the seminal driving experiment of Land and Horwood (1995). Secondly, a human-in-the-loop simulator experiment is performed in which drivers follow both the real-world road and its multisine approximation. Measured steering behaviour on both roads is directly compared, both in the time-domain, using performance and control activity measures, as well as with driver identification results obtained with the multiloop system identification and modeling techniques from Van der El et al. (2019a).

2. MULTISINE SIGNALS

2.1 Driver Identification Problem

This paper presents the work performed under the framework of a larger project in which we aim to increase understanding of driver steering behavior through a *quantitative* measuring and modeling approach (Van der El et al., 2019b). For this work, we investigate the dynamics of drivers' steering behavior in continuous steering tasks, as shown in a block-diagram representation in Fig. 1.

Fig. 1 shows the vehicle dynamics, separated into the steering wheel-to-heading dynamics G_δ^ψ and heading-to-lateral-position dynamics G_ψ^y. Furthermore, the three control responses drivers use when steering through curves

2405-8963
Peer review under responsibility of International Federation of Automatic Control.
10.1016/j.ifacol.2019.12.082

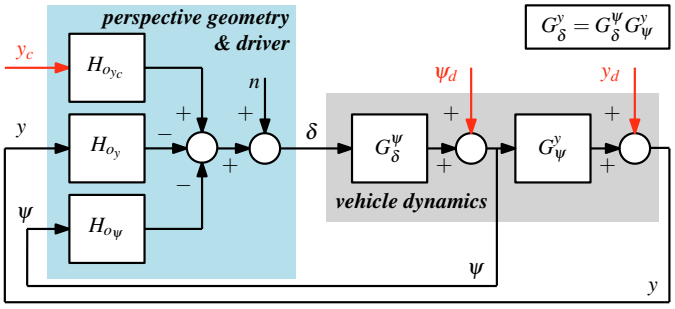

Fig. 1. Illustration of driver steering and multiloop driver dynamics, reproduced from Van der El et al. (2019a).

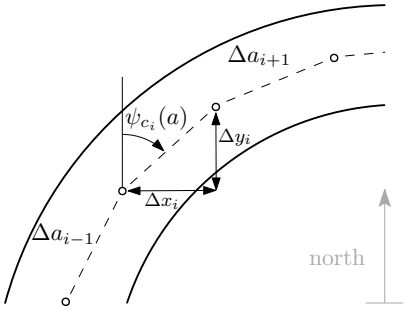

Fig. 2. Road geometry and the commanded heading angle ψ_c as function of along-track distance a.

are indicated: the feedforward (preview) response to the road ahead ($H_{o_{y_c}}$) and feedback responses to the vehicle's heading (H_{o_ψ}) and lateral position (H_{o_y}).

As explained in Van der El et al. (2019a), when using instrumental variable identification techniques to estimate all *three* responses shown in Fig. 1, *three* independent multisine signals, indicated in red, are needed. These are the road geometry y_c and disturbances (i.e., wind-gusts) that perturb the vehicle's heading (ψ_d) and lateral position (y_d). This paper focuses on the first of these signals, by presenting and testing a stepwise methodology for approximating real road geometries with multisine signals.

2.2 Multisine Signal Development

The road reference signal, y_c in Fig. 1, is in practice often defined in terms of the corresponding heading angle reference of the road centerline, ψ_c (Weir and McRuer, 1970), shown in Fig. 2. Here, the road heading is a function of the along-tack distance a, similar to the approach adopted in earlier experiments (Sharp et al., 2000; Lakerveld et al., 2016; Van der El et al., 2018):

$$\psi_c(a) = \sum_{k=1}^{N_f} A[k] \sin\left(\omega[k]a + \phi[k]\right) \tag{1}$$

The signal is characterized by amplitudes $A[k]$, frequencies $\omega[k]$, and phases $\phi[k]$ of the k-th sinusoid, with N_f the number of components. We aim to find the amplitudes, frequencies, and phases such that the multsine signal approximates an original, real-world road geometry best.

In the following, we explain our proposed four-step procedure for approximating real road geometries with a multisine signal as given by Eq. (1). Our proposed procedure is implemented for deriving a multisine signal that matches the road used in the landmark driver steering experiment of Land and Horwood (1995), which used a portion of Queens Drive (QD) in Edinburgh (detailed in personal correspondence).

Step 1: Road Coordinate Extraction To obtain the geometry of a certain stretch of road, a set of (lat/long) coordinates can be extracted from most publicly available navigation databases (e.g., GoogleMaps). First, this raw road coordinate data are converted to measures of distance. The difference in latitude ϕ_i and longitude λ_i (in deg) of two road coordinate points can be converted to relative position coordinates in meters according to:

$$\Delta x_i = \Delta\lambda_i \frac{\pi}{180} R_e \cos\Delta\phi_i \tag{2}$$

$$\Delta y_i = \Delta\phi_i \frac{\pi}{180} R_e \tag{3}$$

Here, R_e indicates the Earth's radius. These equations are valid for a spherical earth approximation, which is acceptable for "small" differences in location, i.e., $[\Delta x, \Delta y] \ll R_e$. The series of $(\Delta x_i, \Delta y_i)$ points fully defines the road geometry, but can be combined through the commanded heading angle:

$$\psi_{c_i} = \arctan\left(\frac{\Delta x_i}{\Delta y_i}\right) \tag{4}$$

The corresponding along-track-distance a is defined as the cumulative sum of the length of all Δa intervals up to the i^{th} road point:

$$a = \sum_{i=1}^{N} \Delta a_i = \sum_{i=1}^{N} \sqrt{\Delta x_i^2 + \Delta y_i^2} \tag{5}$$

These Eqs. (4) and (5) together yield the signal $\psi_c(a)$, which fully defines the road centerline trajectory. The road *curvature*, another common metric for specifying road geometry, is given by $r_c = \frac{d\psi_c}{da}$.

For our application of the above methodology to the segment of Queens Drive in Edinburgh, the acquired road coordinate-data from GoogleMaps consists of a total of $N = 559$ points. With an assumed constant Earth radius of $R_e = 6371$ km, the latitude and longitude coordinates were transformed to the Cartesian road geometry shown in Fig. 3 with the blue markers.

Step 2: Data Processing Exported road coordinates are generally not equally spaced along the length of the road, as is clearly visible for our raw road coordinate data in Fig. 3. An evenly-spaced data point distribution is required for applying the Fourier transform to obtain the road frequency spectrum, and approximating this spectrum with a multisine signal. Therefore, the obtained data are interpolated to constant along-track distance ($\Delta a = 0.1389$ m, corresponding to (Van der El et al., 2019a)) using shape-preserving, piecewise cubic interpolation.

Finally, our experience showed that exported raw road coordinate data contain inaccuracies and artifacts (i.e., noise), which yield unrealistically sharp changes in heading. Therefore, we smoothed the x-, y-coordinate data with a low-pass filter with a 0.007π rad/m normalized cut-off and a 0.05π rad/m stopband frequency (100 dB stopband attenuation). The interpolated and smoothed set

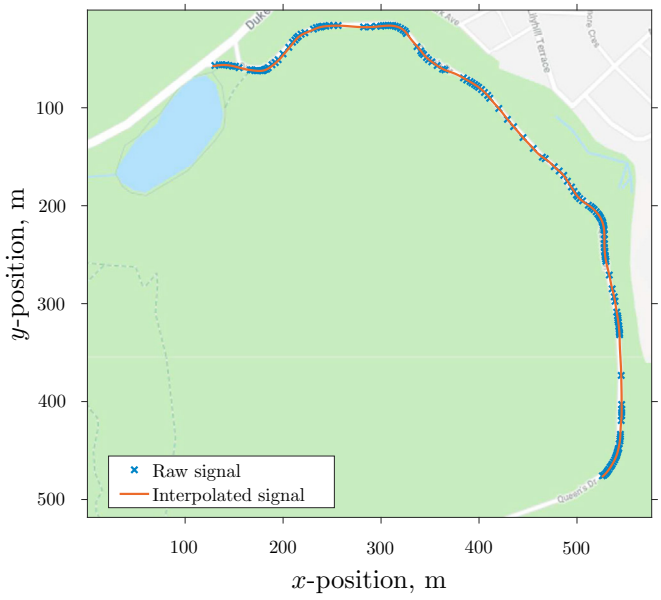

Fig. 3. Top-down map view of the Queens Drive (QD) road segment used by Land and Horwood (1995).

of road points is shown in Fig. 3 in red, and matches the underlying road trajectory well.

Step 3: Road Straightening As is clear from Fig. 2, the considered section of Queens Drive is part of a circular track, meaning that the heading angle has a linear trend (nonzero average curvature). Fig. 4 shows, in blue, this heading ψ_c calculated from the $(\Delta x_i, \Delta y_i)$ coordinates shown in Fig. 3. To follow this road, a nonzero average steering wheel deflection is required. However, a multisine signal lacks such a linear trend, which must thus be removed from the real-world road to capture the *relative* changes in heading (and the required steering) with a multisine signal. To achieve this, the overall road is "straightened" by subtracting the mean curvature of the road from the actual road curvature at each point, yielding the heading angles in Fig. 4 (red line).

Step 4: Multisine Frequency, Amplitude, and Phase Selection Finally, now, the Fourier transform of the heading can be obtained, yielding its frequency spectrum in rad/m, given in blue in Fig. 5. The spectrum reveals that

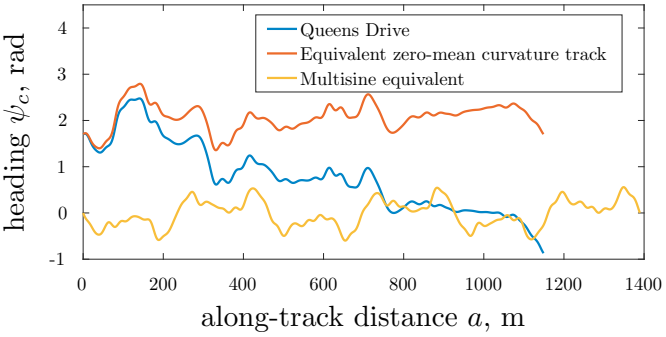

Fig. 4. Heading angle of the real-world road, the same road corrected for the curvature of the circular track and its multisine equivalent.

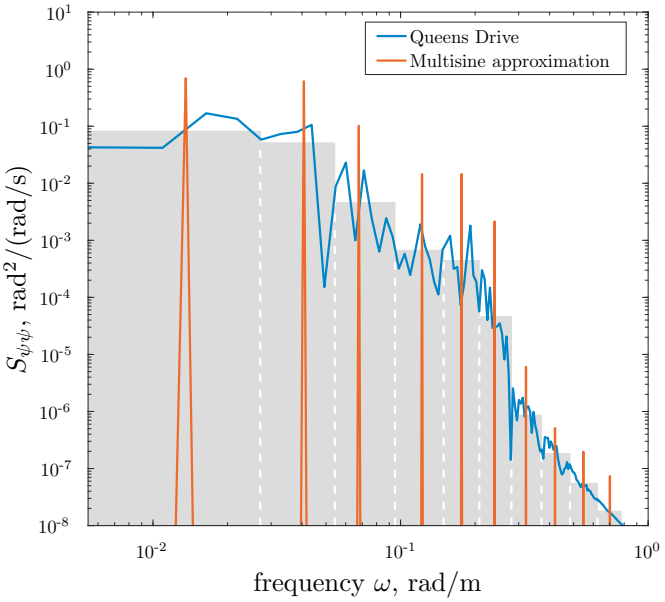

Fig. 5. Road heading signal spectra for the Queens Drive road, and its multisine signal approximation.

the Queens Drive road contains power predominantly at frequencies below 0.25 rad/m. The multisine road signal used in the driving experiments by Van der El et al. (2018, 2019a) was constructed of $N_f = 10$ sine-components, of frequencies up to 0.7 rad/m, to allow measuring the driver's steering dynamics also at higher frequencies. It was decided to approximate the Queens Drive road by a multisine with these same frequencies $\omega[k]$, indicated by the red peaks in Fig. 5. Note that other choices for the frequencies are possible, see (Damveld et al., 2010) for further guidance.

Next, the multisine amplitudes $A[k]$ are determined, by computing the total power of the Queens Drive road in each frequency "bin", with boundaries in the middle between the selected multisine frequencies $\omega[k]$. The bins and total power are indicated by the gray areas in Fig. 5. Each multisine amplitude is then selected such that its power equals the total power in that frequency bin. The resulting multisine signal spectrum is shown in Fig. 5 in red. The phases $\phi[k]$ were subsequently obtained using a brute force method, by generating 10.000 random phase vectors $(-\pi < \phi[k] < \pi)$, and selecting the phase vector for which the heading error variance between the multisine and real-world road signals is smallest. The resulting ψ_c signal, corrected to zero mean, is shown in yellow in Fig. 4, and its characteristics are listed in Table 1.

3. METHODS

To verify whether the multisine (MS) approximation of the original Queens Drive road geometry evokes identical driver steering behavior, a human-in-the-loop experiment was performed in which drivers followed both road trajectories. This experiment was part of a larger study, in which also a replication of the visual occlusion experiment of Land and Horwood (1995) was performed. Here we focus on the verification of the multisine road geometry.

Table 1. Frequencies, amplitudes, and phases of the multisine approximation of the Queens Drive road in Edinburgh. The disturbance signals, reproduced from (Van der El et al., 2018, 2019a), are given for completeness.

	Road center line ψ_c				Heading angle disturbance ψ_d				Lateral position disturbance y_d			
i	k	ω	A	ϕ	k	ω	A	ϕ	k	ω	A	ϕ
-	-	rad/m	deg	rad	-	rad/m	deg	rad	-	rad/m	m	rad
1	3	0.01	16.2	3.96	7	0.03	2.20	5.04	5	0.02	0.29	5.98
2	9	0.04	15.3	3.17	13	0.06	1.74	6.22	11	0.05	0.24	4.04
3	15	0.07	6.20	4.78	23	0.10	1.08	4.17	19	0.09	0.16	3.03
4	27	0.12	2.34	3.40	35	0.16	0.63	4.40	31	0.14	0.09	6.11
5	39	0.18	2.34	6.28	47	0.21	0.41	4.97	43	0.19	0.06	0.99
6	53	0.24	0.90	6.20	65	0.29	0.25	4.97	59	0.27	0.04	0.11
7	71	0.32	0.05	5.42	85	0.38	0.16	4.10	77	0.35	0.02	1.78
8	93	0.42	0.01	5.71	111	0.50	0.11	5.90	101	0.46	0.02	2.28
9	121	0.55	0.01	0.95	143	0.65	0.08	5.48	131	0.59	0.01	0.41
10	155	0.70	0.01	4.79	183	0.83	0.07	0.73	169	0.76	0.01	2.41

3.1 Experiment Setup

The experiment was performed in TU Delft's SIMONA Research Simulator (SRS), see Fig. 6. The motion system of the SRS was not used and participants performed a visual-only driving task, see Fig. 7. Visuals were presented using the collimated 60×40 deg field-of-view outside visual system (single projector), see Fig. 7; the two side projectors of the SRS were switched off to match the experiment of Land and Horwood (1995) as well as possible. Full details of the experimental setup are given in Van der El et al. (2018, 2019a).

The task was performed with a constant forward vehicle velocity $U_0 = 16.9$ m/s, identical to (Land and Horwood, 1995), and the vehicle heading dynamics (G_δ^ψ in Fig. 1) were an integrator, identical to (Land and Horwood, 1995; Van der El et al., 2019a). Vehicle lateral position is obtained by integrating the heading angle. The road was 3 m wide.

For the QD condition the measurement portion of each run covered 1149 m along-track-distance, see Fig. 3. This corresponds to a nominal measurement time of 68 s (when the road centerline is followed perfectly), identical to (Land and Horwood, 1995). For the MS condition, the measurement portion of the road was extended to 1389 m (82.2 s nominal measurement time), identical to (Van der El et al., 2018, 2019a), to guarantee that each sine component fits exactly an integer number of times in the total measurement, for Fourier analysis. The actual trajectory driven by participants in each run was extended by a run-in (277 m) and run-out (138 m) portion, of which the data were not analyzed.

3.2 Experiment Participants and Procedure

Nine male and three female volunteers ($\mu = 25.4$ yr, $\sigma = 3.3$ yr) participated in the experiment. All participants provided informed consent prior to their participation and were in the possession of a valid driver's license ($\mu = 7.2$ yr, $\sigma = 3.0$ yr), with varying travelled distances per year ($\mu = 4420$ km, $\sigma = 7447$ km). Participants were instructed to drive as they would normally do.

They first completed five runs of the QD condition, in which the heading and lateral disturbance signals (ψ_d and y_d) were zero, identical as in (Land and Horwood, 1995). The first two runs were used to familiarize participants with the setup, and only the remaining, final three runs were used for analysis. Subsequently, four runs were performed for the multisine (MS) condition, which *did* include the additional disturbances to facilitate system identification. Here, only a single run was used for practice, and the final three runs were analyzed.

3.3 Dependent Measures

Performance and Control Activity Driver steering on the QD and MS roads is compared by analysis of the measured steering wheel rotations δ (see Fig. 1) and the car's lateral position deviation from the centerline $y_e = y_c - y$. First, measured time traces of δ, as well as the corresponding power spectra, are compared. In addition, the standard deviations of the control output (σ_δ) and

Fig. 6. The SIMONA Research Simulator (SRS).

Fig. 7. Picture of a participant performing the experiment, illustrating the experiment setup.

the lateral position deviations (σ_{y_e}) are used as metrics to compare control activity and road-following performance for both roads. The total variance has four components, e.g., for the control output:

$$\sigma_\delta^2 = \sigma_\delta^2(y_c) + \sigma_\delta^2(y_d) + \sigma_\delta^2(\psi_d) + \sigma_\delta^2(n), \quad (6)$$

which are the variance components at the frequencies of the target centerline (y_c), lateral position disturbance (y_d), heading disturbance (ψ_d), and remnant (n). The separate contributions to the total variance of each component can be computed in the frequency domain, see (Jex et al., 1978) for details. For fair comparison with the disturbance-free QD condition, disturbance-free estimates of σ_δ and σ_{y_e} in the MS condition are obtained by subtracting the two disturbance components (y_d and ψ_d) from the total control output and lateral deviation variances using Eq. (6).

Driver Identification Driver steering in the MS condition is further analyzed using multiloop system identification techniques. The applied methods are identical to those in (Van der El et al., 2019a). The three driver responses to road preview ($H_{o_{y_c}}$), vehicle heading (H_{o_ψ}), and vehicle lateral position (H_{o_y}) are estimated, with the driver steering output (in the frequency domain) defined as the linear combination of the three responses (see also Fig. 1):

$$\delta = H_{o_{y_c}} y_c - H_{o_y} y - H_{o_\psi} \psi \quad (7)$$

First, Frequency-Response Functions (FRFs) are estimated for the three driver responses, and, second, the multiloop driver perception and steering control model from (Van der El et al., 2019a) is fit to the FRF data. Only the first two measurement runs are used for estimating the driver FRFs and models, while the third measurement run is used for validation and for computing the Variance Accounted For (VAF) of the fitted models.

4. RESULTS

4.1 Performance and Control Activity

Fig. 8(a) shows that the measured control outputs for the Queens Drive (QD) road (blue data) and the multisine (MS) task (red data) are clearly different. This is confirmed by the corresponding power spectra in Fig. 8(b). For the multisine road the power spectrum shows distinct peaks at the road and disturbance input frequencies, as expected. In fact, the shape of the power spectrum at the multisine frequencies of the road centerline (black data in Fig. 8(b)) *is identical* to that of the measured control output spectrum in the QD task (blue data). The power at each multisine frequency in the MS task is higher than the power in the QD task, where the power is more spread out across frequencies. For *road following*, it can thus be concluded that the participant shows identical steering behavior on the real road (QD) as compared to the multisine approximation of this road (MS).

This is confirmed in Fig. 9. Both the *total* lateral position deviations and the control outputs (i.e., including the contributions of ψ_d and y_d) are higher on the multisine road, as compared to the Queens Drive road. However, when only considering the centerline and remnant frequencies, so excluding the disturbance components in Eq. (6), the control output and lateral deviation magnitudes are *equivalent* for both roads, for all participants.

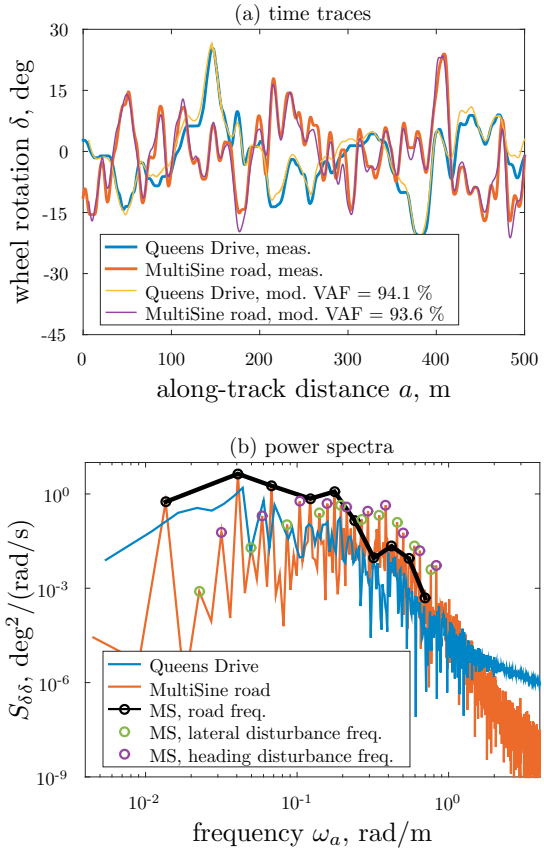

Fig. 8. Measured control output time traces and power spectra (Participant 1, Run 3).

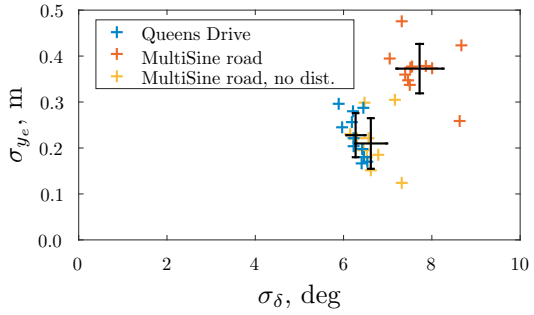

Fig. 9. Measured standard deviations of steering wheel rotations (σ_δ) and lateral deviations from the road centerline (σ_{y_e}), individual participant data and sample average with standard deviations. The multisine road data without disturbances were computed in the frequency domain (Jex et al., 1978).

4.2 Driver Identification

Fig. 10 shows the estimated multiloop driver response dynamics obtained from the MS condition data. Note again that these estimated driver responses can only be obtained because of the three uncorrelated multisine perturbations applied in this task. The estimated FRFs, given by the markers in Fig. 10, show the control dynamics of the driver in response to the road preview, vehicle lateral position, and vehicle heading, respectively. The fitted driver model of Van der El et al. (2019a) evidently captures the driver dynamics very well, except the feedforward

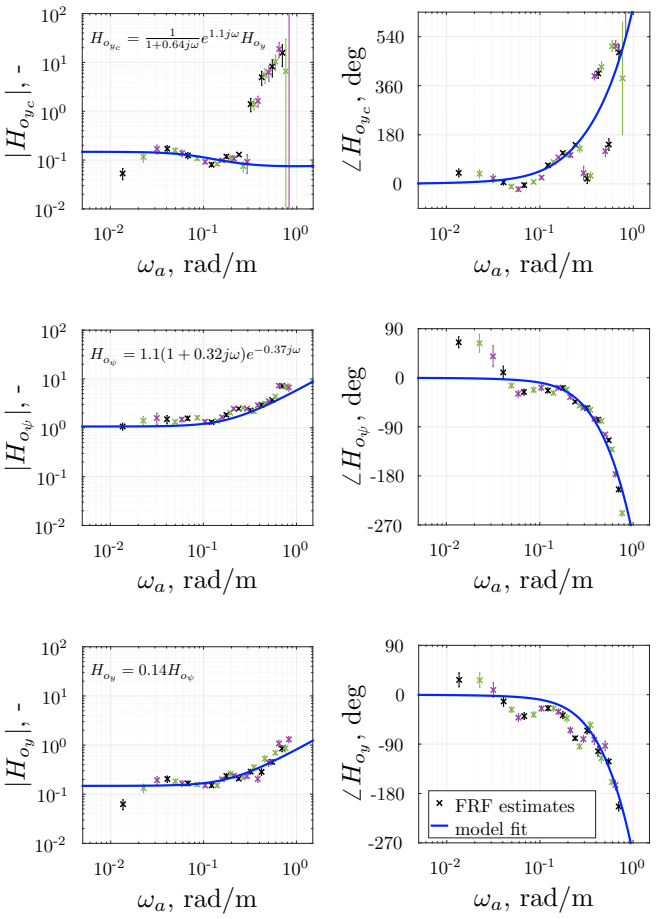

Fig. 10. Example Bode plots of estimated driver dynamics in the MS condition, based on the first two measurement runs of Participant 1.

$H_{o_{y_c}}$ at the highest frequencies, where the control output is low. The FRF estimates thereby validate that the driver model indeed describes the actual driver's multiloop control dynamics.

Using the estimated model to simulate the control output in the third measurement run (validation data) using Eq. (7) yields the "model" time traces in shown in Fig. 8(a) (yellow trace for QD, purple trace for MS). For the multisine road condition, the modeled control outputs are nearly identical to the measured control outputs (red data), with a VAF of 94.1%. Strikingly, using the same estimated model to simulate the control output in the third run of the Queens Drive condition provides an equally good match (93.6% VAF) to the measured control output. Comparable, but slightly noisier results are obtained for the other participants, with average VAFs of 86.5% and 89% in the QD and MS conditions, respectively. These results further indicate that participants adopted equivalent steering behavior in the MS condition, as compared to driving on the corresponding real-world road.

5. CONCLUSION

This paper presented a method to analyze the spectral components of real roads and construct equivalent multisine signals with matched power over selected ranges of frequencies. This method was applied to approximate a portion of Queens Drive in Edinburgh, used in the experiments of Land and Horwood (1995), with a multisine. From collected human-in-the-loop experiment data it was found that driver steering behaviour, in terms of driving performance and driver control dynamics, is equivalent between the real Queens Drive and its multisine approximation. This confirms that a multisine approximation of a real road evokes similar driver behaviour, which enables the application of frequency-domain identification techniques to analyze driver steering behaviour in future curve driving experiments.

REFERENCES

Damveld, H.J., Beerens, G.C., Van Paassen, M.M., and Mulder, M. (2010). Design of forcing functions for the identification of human control behavior. *Journal of Guidance, Control, and Dynamics*, 33(4), 1064–1081.

Donges, E. (1978). A Two-Level Model of Driver Steering Behavior. *Human Factors*, 20(6), 691–707.

Jex, H.R., Magdaleno, R.E., and Junker, A.M. (1978). Roll Tracking Effects of G-vector Tilt and Various Types of Motion Washout. In *Proc. 14th Ann. Conf. on Manual Control*, 463–502.

Lakerveld, P.R., Damveld, H.J., Pool, D.M., Van der El, K., Van Paassen, M.M., and Mulder, M. (2016). The Effects of Yaw and Sway Motion Cues in Curve Driving Simulation. In *Proc. of the 13th IFAC/IFIP/IFORS/IEA Symposium on Analysis, Design, and Evaluation of Human-Machine Systems, Kyoto, Japan.*

Land, M.F. and Horwood, J. (1995). Which Parts of the Road Guide Steering? *Nature*, 377, 339 – 340.

McRuer, D.T., Allen, R.W., Weir, D.H., and Klein, R.H. (1977). New Results in Driver Steering Control Models. *Human Factors*, 19(4), 381–397.

Sharp, R.S., Casanova, D., and Symonds, P. (2000). A Mathematical Model for Driver Steering Control, with Design, Tuning and Performance Results. *Vehicle System Dynamics*, 33(5), 289–326.

Steen, J., Damveld, H.J., Happee, R., Van Paassen, M.M., and Mulder, M. (2011). A Review of Visual Driver Models for System Identification Purposes. In *IEEE International Conference on Systems, Man, and Cybernetics (SMC), 2011*, 2093 – 2100.

Van der El, K., Pool, D.M., Van Paassen, M.M., and Mulder, M. (2019a). A Unifying Theory of Driver Perception and Steering Control on Straight and Winding Roads. *IEEE Trans. on Human-Machine Systems.* Submitted.

Van der El, K., Pool, D.M., and Mulder, M. (2019b). Measuring and Modeling Driver Steering Behavior: From Compensatory Tracking to Curve Driving. *Transportation Research Part F*, 61, 337–346.

Van der El, K., Pool, D.M., Van Paassen, M.M., and Mulder, M. (2018). Identification and Modeling of Driver Multiloop Feedback and Preview Steering Control. In *Proc. of the IEEE International Conference on Systems, Man, and Cybernetics, Myazaki, Japan*, 1227–1232.

Weir, D.H. and McRuer, D.T. (1970). Dynamics of Driver Vehicle Steering Control. *Automatica*, 6(1), 87–98.